

Figure 1. Schematics of the NBP decoder. The main cycle in the gray box is repeated  $N_c$  times. Inside one cycle there are two phases of computation, the  $cv \rightarrow vc$  and  $vc \rightarrow cv$  phases which are governed by Eqs. (4) and (5) respectively. The inputs to the neural network are denoted by the green boxes, where the prior and syndrome correspond to  $\{l_v\}$  in Eq. (4) and  $\{s_c\}$  in Eq. (5) respectively. After each cycle, the set of output  $\{\mu_{c \rightarrow v}\}$  is marginalized by Eq. (6) and the resulting  $\{\mu_v\}$  is sent to the loss function Eq. (8). We also introduce residual connections to facilitate training of deep networks [37]. (See SM for details.)

equations:

$$\mu_{v \rightarrow c}^{(t+1)} = l_v + \sum_{c' \in \mathcal{N}(v) \setminus c} \mu_{c' \rightarrow v}^{(t)}, \quad (1)$$

$$\mu_{c \rightarrow v}^{(t+1)} = (-1)^{s_c} 2 \tanh^{-1} \prod_{v' \in \mathcal{N}(c) \setminus v} \tanh \frac{\mu_{v' \rightarrow c}^{(t)}}{2}, \quad (2)$$

where  $l_v = \log \left( \frac{P(e_v=0)}{P(e_v=1)} \right)$  is the prior log-likelihood ratio for variable  $e_v$  and  $\mathcal{N}(x) \setminus y$  is the set of all neighbors of  $x$  except for  $y$  [4]. The initial condition for the iteration is  $\mu_{v \rightarrow c}^{(t=0)} = 0$ , and after  $T$  steps (sufficiently long), one stops the iteration and performs the following marginalization for the posterior log-likelihood ratio:

$$\mu_v = l_v + \sum_{c \in \mathcal{N}(v)} \mu_{c \rightarrow v}^{(T)}. \quad (3)$$

The posterior marginal probability relates to  $\mu_v$  according to  $\log \left( \frac{P(e_v=0|\mathbf{s})}{P(e_v=1|\mathbf{s})} \right) = \mu_v$ . Equivalently  $P(e_v = 1|\mathbf{s}) = \sigma(\mu_v)$  and  $P(e_v = 0|\mathbf{s}) = 1 - \sigma(\mu_v)$ , where  $\sigma(x) = 1/(e^x + 1)$  is the Fermi function (or horizontally-flipped sigmoid function). The inferred error pattern maximizes these marginal probabilities, i.e.,  $e_v$  is inferred to be 0/1 when  $\mu_v$  is positive/negative.

*Neural belief propagation.* — The above iterative procedure can be exactly mapped to a deep neural network, where each neuron represents a message  $\mu_{c \rightarrow v}$  or  $\mu_{v \rightarrow c}$  [15]. (See Fig. 1.) This permits generalization of the original BP algorithm by introducing additional “trainable” weights  $w_{c'v,vc}^{(t)}$  and  $w_{cv,v}^{(T)}$ , and “trainable” biases  $b_v^{(t)}$  and  $b_v^{(T)}$ . Specifically, in this NBP algorithm, Eqs. (1, 2,

3) are modified to:

$$\mu_{v \rightarrow c}^{(t+1)} = l_v b_v^{(t)} + \sum_{c' \in \mathcal{N}(v) \setminus c} \mu_{c' \rightarrow v}^{(t)} w_{c'v,vc}^{(t)}, \quad (4)$$

$$a \left( \mu_{c \rightarrow v}^{(t+1)} \right) = i\pi s_c + \sum_{v' \in \mathcal{N}(c) \setminus v} a \left( \mu_{v' \rightarrow c}^{(t)} \right), \quad (5)$$

$$\mu_v = l_v b_v^{(T)} + \sum_{c \in \mathcal{N}(v)} \mu_{c \rightarrow v}^{(T)} w_{cv,v}^{(T)}, \quad (6)$$

respectively [15, 38]. Notice that all equations above have the form of weighted sum plus bias, interleaved with the nonlinear function  $a(x) = \log(\tanh(x/2))$ . This is the canonical form of feed-forward neural networks [39]. When setting all newly introduced parameters to 1, these equations became the standard BP equations [40].

To train these weights, one minimizes a carefully designed loss function  $\mathcal{L}$  by back-propagating its gradients w.r.t. all trainable parameters. E.g., biases are updated according to  $\Delta b_v^{(t)} = -lr \times \partial \mathcal{L} / \partial b_v^{(t)}$ , where  $lr$  is the learning rate. For classical codes, one aims for reproducing the whole error pattern exactly, so the natural choice of the loss function is the binary cross entropy function between the inferred error pattern and the true error pattern:

$$\mathcal{L}(\vec{\mu}; \mathbf{e}) = - \sum_v e_v \log \sigma(\mu_v) + (1 - e_v) \log [1 - \sigma(\mu_v)]. \quad (7)$$

*Quantum setting.* — Quantum noise can be modeled by random Pauli operators  $I$ ,  $\hat{X}$ ,  $\hat{Y}$ , and  $\hat{Z}$  on the qubits. A convenient way of bookkeeping a  $N$ -qubit error uses a  $2N$ -bit string  $\mathbf{e}$  representing the Pauli operator:  $\hat{\mathcal{P}}(\mathbf{e}) = \prod_{1 \leq i \leq N} [\hat{X}_i]^{e_i} [\hat{Z}_i]^{e_{i+N}}$ . In this representation, two Pauli-strings operators  $\hat{\mathcal{P}}(\mathbf{a})$  and  $\hat{\mathcal{P}}(\mathbf{b})$  commute/anticommute when  $\mathbf{a}^T M \mathbf{b}$  is even/odd, where the symplectic inner product is defined with  $M = \begin{pmatrix} & 1_{N \times N} \\ 1_{N \times N} & \end{pmatrix}$ . Note that all Pauli-string operators satisfy  $\hat{\mathcal{P}}^2 = 1$ .

Likewise, the quantum codewords  $|\psi\rangle$  are defined by a set of constraints  $S_j |\psi\rangle = +|\psi\rangle$  where each stabilizer generator  $S_j$  is a Pauli-string operator. For these equations to have a solution, it is necessary for the  $S_j$  to mutually commute and to not generate  $-1$  under multiplication. Using the above bookkeeping, we can represent each stabilizer generator  $S_j$  by a  $2N$ -bit string, and assemble these strings as rows of a parity-check matrix  $H$ . A quantum LDPC code is one whose parity-check matrix is row- and column-sparse.

There is a crucial difference between classical and quantum error correction. In the classical case, successful decoding means the inferred error  $\mathbf{e}^{\text{inf.}}$  is exactly the same as the true error  $\mathbf{e}$ ; while in the quantum case, one only requires the total error  $\mathbf{e}^{\text{tot.}} = \mathbf{e} + \mathbf{e}^{\text{inf.}} \pmod{2}$  to belong to the “stabilizer group” – the set of all Pauli-string operators spanned by the rows of  $H$ . This is because two

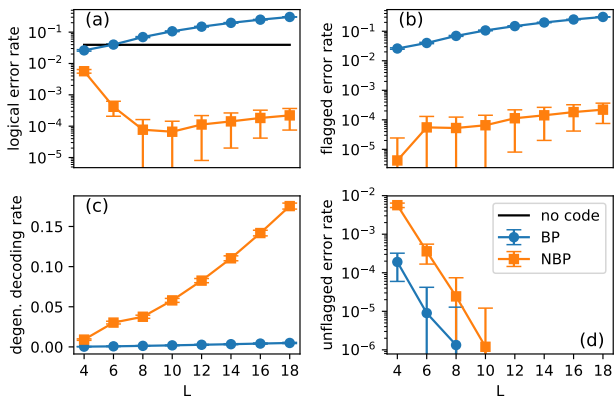


Figure 2. Training the NBP decoder for the toric code with different code sizes. (a) The logical error rate decreases substantially after training (tested at  $p_{err} = 0.01$ ). Here the logical error rate is broken up into two terms in (b) and (d), corresponding to “flagged” and “unflagged” errors, respectively. (See main text for details.) (c) The NBP decoder exploits degeneracy by correctly decoding with an error pattern that is not exactly the same as the true error pattern. Training parameters:  $N_c = 25$ ,  $lr = 2 \times 10^{-4}$ .

Pauli-string operators  $E$  and  $F = ES_j$  that differ by a stabilizer have identical action on all codestates. To test if  $\mathbf{e}^{\text{tot.}}$  belongs to the stabilizer group, one simply needs to check that it commutes with all the operators that commute with the stabilizers, i.e., that  $H^\perp M \mathbf{e}^{\text{tot.}} = \mathbf{0} \pmod 2$  where  $H^\perp$  is the matrix that generates the orthogonal complement of  $H$  with respect to the symplectic inner product,  $HM(H^\perp)^T = \mathbf{0} \pmod 2$ .

The above analysis motivates the design the following loss function tailored for quantum error correction:

$$\mathcal{L}(\vec{\mu}; \mathbf{e}) = \sum_i f \left( \sum_{jk} H_{ij}^\perp M_{jk} [e_k + \sigma(\mu_k)] \right). \quad (8)$$

Note the parity check  $\text{parity}(x) = x \pmod 2$  is replaced by the continuous and differentiable function  $f(x) = |\sin(\pi x/2)|$  to facilitate gradient-based machine-learning techniques. This loss is minimized when the true error  $\mathbf{e}$  and the inferred error  $\mathbf{e}^{\text{inf.}}$  sum to a stabilizer.

The loss function can also be averaged over all NBP-cycles  $\bar{\mathcal{L}} = \frac{1}{N_c} \sum_{i=1}^{N_c} \mathcal{L}(\vec{\mu}^{(i)}; \mathbf{e})$ , which requires marginalization after each cycle. In this work we use a variation of this form. See SM for more details.

*Toric code.*— We first study the toric code [36] on an  $L \times L$  square lattice, which is a simple and widely studied quantum LDPC. (See Fig. 3 for the local Tanner graph.) During training, we generate error patterns consisting of independent  $X$  and  $Z$  errors with physical error rate  $p_{err}$ , i.e.,  $P(e_v = 1) = p_{err}$  for all  $v$ . In each minibatch, 120 error patterns are drawn from 6 physical error rates that are uniformly distributed in the range  $p_{err} \in [0.01, 0.05]$ .

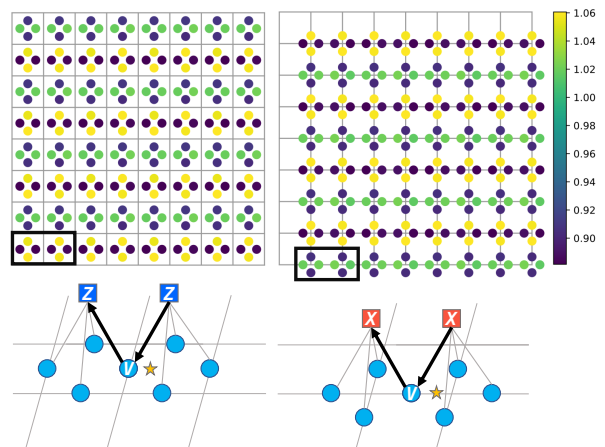


Figure 3. (Top panels) One of the observed patterns of the learned weights for the toric code. To obtain this clear pattern, we implemented weights sharing (see main text) with  $\mathbf{G} = (2i, 2j)$ ,  $i, j = 0, 1, \dots$ . A noisy version of the same pattern is observed when weight sharing is turned off. (Bottom panels) Tanner graph of the toric code and the position of  $cvvc$  weights (yellow star). Correspondence to the top panels is marked by the black box.

After  $\sim 10000$  minibatches, we test the performance of the trained decoder. Figure 2 compares the original BP decoder (before training) and the trained NBP decoder at  $p_{err} = 0.01$  for various code sizes. Training significantly enhances decoding accuracy up to three orders of magnitude (Fig. 2a), and we observe that the training time required for convergence depends weakly on the code size  $L$ . (See SM for details.)

We can distinguish two types of decoding failure. “Flagged” failures occur when the correction inferred by the decoder does not return the system to the code space – there remains a non-trivial syndrome after decoding. “Unflagged” failures occur when the correction returns the system to the wrong code state. These two contributions to the overall logical error rate are shown in Fig. 2b and 2d, respectively. We observe that training greatly reduces flagged failures at the expense of slightly increasing unflagged failures, and overall there is a significant net decrease of failures. It should be noted that flagged failures are benign because they can be re-decoded, using either a more accurate but more expensive decoder (e.g. the minimum-weight perfect matching [41]) or a higher layer of code for erasure errors. Such a mixed decoding strategy would combine the speed and flexibility of BP decoder and reliability of a more expensive decoder used on a very small fraction (e.g.  $10^{-4}$ ) of instance.

The loss function Eq. (8) takes into account error degeneracy, and we see on Fig. 2c that the frequency of successful decoding where the actual and the inferred error differ by a stabilizer increases with the code length. This rate was nearly zero with the untrained decoder (see

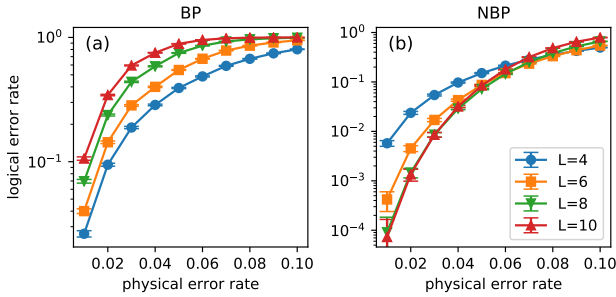


Figure 4. Evolution of the logical error rate as a function of the physical error rate, for the BP/NBP decoder before/after training. (a) Before training the performance of the BP decoder is worse for larger code sizes at all physical error rates. (b) After training, the performance improves substantially for all code sizes at all physical error rates, and the performance curves start to cross each other. This indicates the development of a threshold.

SM for examples of learned stabilizers).

The periodic nature of the toric code inspired us to utilize a weight-sharing technique, where the weights  $w_{c'_1 v_1, v_1 c_1}$  and  $w_{c'_2 v_2, v_2 c_2}$  are invariant under lattice translation  $\mathbf{G}$ . We can control the amount of sharing by the size of  $\mathbf{G}$  (similar to the filter-size in convolutional neural networks). Fig. 3 is a graphical representation of the trained weights, and suggests that symmetry breaking improves BP for quantum codes. We also observe that weights trained on one code size can also increase the performance when applied to codes of different sizes, which implies that the learning is universal/transferable (see SM for more details).

Figure 4 shows that significant improvement can be achieved across a range of physical error rates. Using the original BP, increasing the code size leads to worse performance. After training, performance improves with size for sufficiently low error rates, and the trend indicates that further improved training might lead to a BP decoder with a finite threshold.

When the neural network is initialized away from BP, training gets stuck at a much worse local minimum. This illustrates the importance of incorporating domain knowledge (when possible) before using general machine-learning methods as black boxes, which contrasts with prior uses of neural net decoding of the toric code [16, 18].

*Quantum LDPC codes with high rate.*— The toric code encodes a constant number  $K = 2$  of qubits in a growing number  $N$  of physical qubits, thus achieving a vanishing rate  $r = K/N$ . We now turn to quantum LDPC codes with constant rates.

The quantum bicycle code [5] is a quantum LDPC code constructed from a random binary vector  $\mathbf{A}$  of size  $N/2$ . First, all cyclic permutations of  $\mathbf{A}$  are collected as columns in a matrix  $C$ . Then  $C$  is concatenated with its transpose to form  $H_0 = [C, C^T]$ , from which  $K/2$

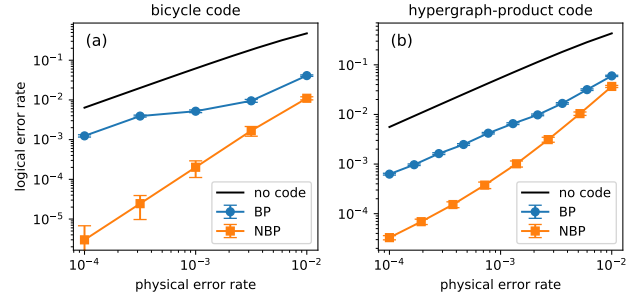


Figure 5. Training greatly improves the BP decoder for quantum LDPC codes with high rates. (a) Quantum bicycle code with code parameter  $[[256, 32]]$  and rate  $r = 0.125$ . Training parameters:  $N_c = 12$ ,  $lr = 1 \times 10^{-4}$ . (b) Quantum hypergraph-product code with code parameter  $[[129, 28]]$  and rate  $r \sim 0.2$ . Training parameters:  $N_c = 12$ ,  $lr = 1 \times 10^{-4}$ .

rows are chosen randomly and removed. After these constructions,  $H_0$  is a self-dual matrix (meaning  $H_0 H_0^T = 0 \pmod{2}$ ) of size  $(N - K)/2 \times N$ . The final parity-check matrix for the quantum bicycle code is  $H = \begin{pmatrix} H_0 \\ H_0 \end{pmatrix}$ . The sparsity of this matrix can be controlled by the number of nonzero elements in  $\mathbf{A}$ . Training the NBP decoder for a quantum bicycle code with  $N = 256$ ,  $K = 32$  and  $\sum_i A_i = 8$  improves the accuracy up to 3 orders of magnitude (Fig. 5a).

The quantum hypergraph-product code [6] is constructed from two classical codes with parity-check matrices  $[H_1]_{m_1 \times n_1}$  and  $[H_2]_{m_2 \times n_2}$ . The following products are constructed  $H_X = [H_1 \otimes I_{n_2 \times m_2}, I_{m_1 \times n_1} \otimes H_2^T]$  and  $H_Z = [I_{n_1 \times m_1} \otimes H_2, H_1^T \otimes I_{m_2 \times n_2}]$ , and the parity-check matrix of the quantum code follows  $H = \begin{pmatrix} H_X \\ H_Z \end{pmatrix}$ , which performs  $m = m_1 n_2 + n_1 m_2$  checks on  $n = m_1 m_2 + n_1 n_2$  qubits. In this paper, we study a hypergraph-product code, for which  $H_1$  and  $H_2$  are the classical  $[7, 4, 3]$  and  $[15, 7, 5]$  BCH codes, respectively. This code has rate  $r = 28/129 \sim 0.2$ . Training the NBP decoder for this code improves the accuracy up to one order of magnitude (Fig. 5b).

*Conclusions.*— We significantly improved the belief-propagation decoders for quantum LDPC codes by training them as deep neural networks. Our results on the toric code, the quantum bicycle code and the quantum hypergraph-product code all show orders of magnitude of enhancement in decoding accuracy. The original belief propagation is known to have bad performance for quantum error-correcting codes [8]. On the other hand, training a neural decoder with general architecture has been reported to be hard for large codes [20, 42]. Our results indicate that combining the general framework of machine learning and the specific domain knowledge of quantum error correction is a promising approach, when neither works well individually.

The significance of this result is supported by the tremendous success of BP with classical LDPC codes [4], and the fact that quantum LDPC codes promise a low-overhead fault-tolerant quantum computation architecture [34]. In addition, our techniques could be adapted to uses of BP in other quantum many-body problems, such as improving the quantum cavity method [11–14].

*Acknowledgments.*— Y.H.L would like to thank helpful discussions with Pavithran Iyer, Anirudh Krishna, Xin Li, Alex Rigby, and Colin Trout. Special thanks go to Liang Jiang and Stefan Krastanov, who shared similar ideas. This research was undertaken thanks in part to funding from the Canada First Research Excellence Fund. Computations were made on the supercomputer Helios managed by Calcul Québec and Compute Canada. The operation of this supercomputer is funded by the Canada Foundation for Innovation (CFI), the ministère de l'Économie, de la science et de l'innovation du Québec (MESI) and the Fonds de recherche du Québec - Nature et technologies (FRQ-NT). We used TensorFlow [43] to build and train neural belief-propagation decoders.

- 
- [1] M Mezard, G Parisi, and M Virasoro, *Spin Glass Theory and Beyond*, World Scientific Lecture Notes in Physics, Vol. 9 (WORLD SCIENTIFIC, 1986).
- [2] Judea Pearl, “Reverend Bayes on inference engines: A distributed hierarchical approach,” *Proc. Second Natl. Conf. Artif. Intell. AAAI-82*, 133–136 (1982).
- [3] R. G Gallager, “Low-density parity-check codes,” *IEEE Trans. Inf. Theory* **8**, 21–28 (1962).
- [4] Tom Richardson and Ruediger Urbanke, *Modern Coding Theory* (Cambridge University Press, Cambridge, 2008).
- [5] D.J.C. MacKay, Graeme Mitchison, and P.L. McFadden, “Sparse-Graph Codes for Quantum Error Correction,” *IEEE Trans. Inf. Theory* **50**, 2315–2330 (2004).
- [6] Jean-Pierre Tillich and Gilles Zemor, “Quantum LDPC Codes With Positive Rate and Minimum Distance Proportional to the Square Root of the Blocklength,” *IEEE Trans. Inf. Theory* **60**, 1193–1202 (2014).
- [7] Anthony Leverrier, Jean-Pierre Tillich, and Gilles Zemor, “Quantum Expander Codes,” in *2015 IEEE 56th Annu. Symp. Found. Comput. Sci.*, Vol. 2015-Decem (IEEE, 2015) pp. 810–824.
- [8] David Poulin and Yeojin Chung, “On the iterative decoding of sparse quantum codes,” [arXiv:0801.1241](https://arxiv.org/abs/0801.1241) (2008).
- [9] Yun-Jiang Wang, Barry C Sanders, Bao-ming Bai, and Xin-mei Wang, “Enhanced Feedback Iterative Decoding of Sparse Quantum Codes,” *IEEE Trans. Inf. Theory* **58**, 1231–1241 (2012).
- [10] Zunaira Babar, Panagiotis Botsinis, Dimitrios Alanis, Soon Xin Ng, and Lajos Hanzo, “Fifteen Years of Quantum LDPC Coding and Improved Decoding Strategies,” *IEEE Access* **3**, 2492–2519 (2015).
- [11] M. B. Hastings, “Quantum belief propagation: An algorithm for thermal quantum systems,” *Phys. Rev. B* **76**, 201102 (2007).
- [12] David Poulin and Ersen Bilgin, “Belief propagation algorithm for computing correlation functions in finite-temperature quantum many-body systems on loopy graphs,” *Phys. Rev. A* **77**, 052318 (2008).
- [13] C. Laumann, A. Scardicchio, and S. L. Sondhi, “Cavity method for quantum spin glasses on the Bethe lattice,” *Phys. Rev. B* **78**, 134424 (2008).
- [14] David Poulin and Matthew B Hastings, “Markov Entropy Decomposition: A Variational Dual for Quantum Belief Propagation,” *Phys. Rev. Lett.* **106**, 080403 (2011).
- [15] Eliya Nachmani, Yair Be’ery, and David Burshtein, “Learning to decode linear codes using deep learning,” in *2016 54th Annu. Allert. Conf. Commun. Control. Comput.* (IEEE, 2016) pp. 341–346.
- [16] Giacomo Torlai and Roger G. Melko, “Neural Decoder for Topological Codes,” *Phys. Rev. Lett.* **119**, 030501 (2017).
- [17] Paul Baireuther, Thomas E. O’Brien, Brian Tarasinski, and Carlo W. J. Beenakker, “Machine-learning-assisted correction of correlated qubit errors in a topological code,” *Quantum* **2**, 48 (2018).
- [18] Stefan Krastanov and Liang Jiang, “Deep Neural Network Probabilistic Decoder for Stabilizer Codes,” *Sci. Rep.* **7**, 11003 (2017).
- [19] Savvas Varsamopoulos, Ben Criger, and Koen Bertels, “Decoding small surface codes with feedforward neural networks,” *Quantum Sci. Technol.* **3**, 015004 (2018).
- [20] Nishad Maskara, Aleksander Kubica, and Tomas Jochym-O’Connor, “Advantages of versatile neural-network decoding for topological codes,” [arXiv:1802.08680](https://arxiv.org/abs/1802.08680) (2018).
- [21] Christopher Chamberland and Pooya Ronagh, “Deep neural decoders for near term fault-tolerant experiments,” *Quantum Sci. Technol.* **3**, 044002 (2018).
- [22] Thomas Fösel, Petru Tighineanu, Talitha Weiss, and Florian Marquardt, “Reinforcement Learning with Neural Networks for Quantum Feedback,” [arXiv:1802.05267](https://arxiv.org/abs/1802.05267) (2018).
- [23] Amarsanaa Davaasuren, Yasunari Suzuki, Keisuke Fujii, and Masato Koashi, “General framework for constructing fast and near-optimal machine-learning-based decoder of the topological stabilizer codes,” [arXiv:1801.04377](https://arxiv.org/abs/1801.04377) (2018).
- [24] P. Baireuther, M. D. Caio, B. Criger, C. W. J. Beenakker, and T. E. O’Brien, “Neural network decoder for topological color codes with circuit level noise,” [arXiv:1804.02926](https://arxiv.org/abs/1804.02926) (2018).
- [25] Nikolas P. Breuckmann and Xiaotong Ni, “Scalable Neural Network Decoders for Higher Dimensional Quantum Codes,” *Quantum* **2**, 68 (2017).
- [26] Xiaotong Ni, “Neural Network Decoders for Large-Distance 2D Toric Codes,” [arXiv:1809.06640](https://arxiv.org/abs/1809.06640) (2018).
- [27] Ryan Sweke, Markus S. Kesselring, Evert P. L. van Nieuwenburg, and Jens Eisert, “Reinforcement learning decoders for fault-tolerant quantum computation,” [arXiv:1810.07207](https://arxiv.org/abs/1810.07207) (2018).
- [28] Sergey Bravyi, Martin Suchara, and Alexander Vargo, “Efficient algorithms for maximum likelihood decoding in the surface code,” *Phys. Rev. A* **90**, 032326 (2014).
- [29] Andrew S. Darmawan and David Poulin, “Linear-time general decoding algorithm for the surface code,” *Phys. Rev. E* **97**, 051302 (2018).
- [30] Nicolas Delfosse and Naomi H. Nickerson, “Almost-linear time decoding algorithm for topological codes,” [arXiv:1709.06218](https://arxiv.org/abs/1709.06218) (2017).
- [31] Guillaume Duclos-Cianci and David Poulin, “Fast De-

- coders for Topological Quantum Codes,” *Phys. Rev. Lett.* **104**, 050504 (2010).
- [32] Omar Fawzi, Antoine Grosseppellier, and Anthony Leverrier, “Efficient decoding of random errors for quantum expander codes,” [arXiv:1711.08351](#) (2017).
- [33] Antoine Grosseppellier and Anirudh Krishna, “Numerical study of hypergraph product codes,” [arXiv:1810.03681](#) (2018).
- [34] Daniel Gottesman, “Fault-tolerant quantum computation with constant overhead,” *Quant. Info. and Comp.* **14**, 1338 (2014).
- [35] Omar Fawzi, Antoine Grosseppellier, and Anthony Leverrier, “Constant overhead quantum fault-tolerance with quantum expander codes,” [arXiv:1808.03821](#) (2018).
- [36] Alexei Kitaev, “Anyons in an exactly solved model and beyond,” *Ann. Phys. (N. Y.)* **321**, 2–111 (2006).
- [37] Kaiming He, Xiangyu Zhang, Shaoqing Ren, and Jian Sun, “Deep Residual Learning for Image Recognition,” [arXiv:1512.03385](#) (2015).
- [38] Henk Wymeersch, Federico Penna, and Vladimir Savic, “Uniformly reweighted belief propagation: A factor graph approach,” in *2011 IEEE Int. Symp. Inf. Theory Proc.*, 2 (IEEE, 2011) pp. 2000–2004.
- [39] I Goodfellow, Y Bengio, and A Courville, *Deep Learning* (MIT Press, 2016).
- [40] For numerical stability, argument of  $\tanh^{-1}(\cdot)$  is truncated to  $(-1 + \epsilon, 1 - \epsilon)$  and we choose  $\epsilon = 10^{-4}$ . Decreasing  $\epsilon$  does not change the main conclusion of the paper.
- [41] J. Edmonds, “Paths, trees and flowers,” *Canad. J. Math.* **17** (1965).
- [42] Tobias Gruber, Sebastian Cammerer, Jakob Hoydis, and Stephan ten Brink, “On Deep Learning-Based Channel Decoding,” [arXiv:1701.07738](#) (2017).
- [43] Martín Abadi, Ashish Agarwal, Paul Barham, Eugene Brevdo, Zhifeng Chen, Craig Citro, Greg S. Corrado, Andy Davis, Jeffrey Dean, Matthieu Devin, Sanjay Ghemawat, Ian Goodfellow, Andrew Harp, Geoffrey Irving, Michael Isard, Yangqing Jia, Rafal Jozefowicz, Lukasz Kaiser, Manjunath Kudlur, Josh Levenberg, Dan Mane, Rajat Monga, Sherry Moore, Derek Murray, Chris Olah, Mike Schuster, Jonathon Shlens, Benoit Steiner, Ilya Sutskever, Kunal Talwar, Paul Tucker, Vincent Vanhoucke, Vijay Vasudevan, Fernanda Viegas, Oriol Vinyals, Pete Warden, Martin Wattenberg, Martin Wicke, Yuan Yu, and Xiaoqiang Zheng, “TensorFlow: Large-Scale Machine Learning on Heterogeneous Distributed Systems,” [arXiv:1603.04467](#) (2016).